

The Flexural Behavior of One-Way Concrete Bubbled Slabs Reinforced by GFRP-Bars with Embedded Steel I-Sections

Mohannad Abdulkhaliq

Department of Civil Engineering, College of Engineering, University of Baghdad, Iraq
mohannad.abd2101m@coeng.uobaghdad.edu.iq (corresponding author)

Ali Hussein Al-Ahmed

Department of Civil Engineering, College of Engineering, University of Baghdad, Iraq
dr.ali-alahmed@coeng.uobaghdad.edu.iq

Received: 29 April 2024 | Revised: 27 May 2024 and 31 May 2024 | Accepted: 16 June 2024

Licensed under a CC-BY 4.0 license | Copyright (c) by the authors | DOI: <https://doi.org/10.48084/etasr.7680>

ABSTRACT

This study examines the behavior of polymer bubbled deck slab systems, one-way concrete slabs with polymer sphere voids reinforced with Glass Fiber-Reinforced Polymer (GFRP) rebars, and embedded I-shaped steel beams. Six one-way structural concrete slabs (2600 mm long, 600 mm wide, 150 mm deep) were tested and directly supported under two points bending. Five Bubbled Slabs (BS), one of which was un-strengthened, were compared to the reference Solid Slab (SS) without polymer spheres. Each slab had 95 polymer sphere voids of 90 mm diameter and 15.48% self-weight decrease. Several parameters, including specimen type (SS or BS) and internal strengthening, were optimized using steel I-shapes in two distinct forms (2 and 4 pcs. of steel I-sections). Channel Shear Connectors (CSCs) and bent-up steel bars (10 mm in diameter) were implemented to increase shear resistance, with the 4I-section form having a cross-sectional area equivalent to the 2I-section form. In contrast to the SS, the BS exhibited a wider range of deformations during the same loading stage, with ultimate load capacity decreasing by 30% and deflection occurring at a greater ratio of approximately 18% to 85%. Additionally, the embedded steel I-shapes improved specimen performance compared to BS and SS. This occurred by reducing deflection at a service load by 60% and 49%, eliminating cracks, improving ultimate load capacity by 85% and 30%, and enhancing flexural stiffness by 102% and 71%, respectively, at the ultimate loading stage. CSC increased ultimate load by 13% to 22% and deflection by 8% to 15%, compared to specimens without CSC.

Keywords-Glass Fiber-Reinforced Polymer (GFRP) bars; embedded steel I-sections; bubbled slabs; flexural strength; one-way slabs; spherical voids; internal strengthening; deflection

I. INTRODUCTION

Buildings need blocks, or slabs, for structural support. They create spaces in structures and require a lot of concrete. Slabs must be employed and designed efficiently to guarantee stability and strength. To reduce the amount of concrete utilized, slab design must be optimized because using more concrete than needed may increase costs and resource utilization [1]. Many attempts have been made to lighten concrete slabs without decreasing flexural strength. Given that aggregate interlock is crucial for shear resistance, not all internal concrete can be replaced, while the presence of the latter in the upper section of the slab is necessary to create a compression block that provides resistance against flexural tension. Additionally, concrete in the tension zone is required to establish a strong bond with the reinforcement for resistance purposes. Also, the slab's upper and lower faces must be connected to work together and transfer stresses [2-5]. Bubble

Deck is an innovative floor slab weight reduction method that removes non-structural concrete from its center. Using void formers in the slab's core reduces its weight by 35%. As the dead load decreases, reinforcing needs are reduced, decreasing structural steel. Optimizing foundation design for lower dead loads decreases construction time and material costs [6-10]. Research and testing demonstrate that slabs, including internal spherical spaces, have 87% of the flexural stiffness of the SS. This means that a slab with voids may flex or deform more at the serviceable point than an SS. However, the material's stiffness-to-bending resistance ratio determines deflection. Steel-reinforced concrete buildings have been used in several infrastructure types for over a century. Steel reinforcement corrodes quickly in hostile environments, especially maritime ones. Corrosion, reduced structure lifetime, and structural collapse can render maintenance and repair expensive. Modern polymer technology has generated the latest Fiber-Reinforced Polymer (FRP) reinforcing bars, especially the GFRP ones.

Steel reinforcement is replaced by corrosion-resistant GFRP bars in structural concrete applications. These materials are ideal for tough steel reinforcing situations since they do not corrode [12-15]. GFRP bars have become more important in the past decade for achieving RC construction standards due to their low weight, quick setup and maintenance, corrosion-proof, and excellent tensile strength [16-27]. Despite its tensile stress endurance, its low cost, and its lightweight nature, FRP's use is limited. Only a few studies have strengthened BS with FRP [28-30].

Authors in [30] evaluated fifteen 1000 mm × 1000 mm Reinforced Concrete (RC) square slabs with plastic spherical gaps for flexural capacity. The ultimate load capacity of a BS (ball diameter to slab's thickness ratio $B/H=0.80$) is 90 to 100% of that of an SS. Authors in [29] studied bubble deck slabs reinforced with GFRP sheets and elliptical balls under uniform load. Finite Element Analysis (FEA) with ANSYS software was used to analyze slabs and reduce deformation. The study compared bubble deck slabs with and without GFRP sheets for total deformation, directional deformation, and equivalent stress. The numerical modeling used (1730 1350 × 230 mm bubble deck slabs and a 180 × 240 mm elliptical void. This space was filled with High-Density Polyethylene (HDPE) elliptical balls. Compared to bubble deck slabs with elliptical balls alone, GFRP sheets improve load-carrying capacity and reduce deflection. Additional studies were conducted in [31] on seven 700 × 450 × 80 mm air-bubbled RC slabs. After burning and loading the slabs until they failed, CFRP strips were applied to fix them, while one slab was kept as a reference. The recovered BSs have flexural strength similar to that of the reference sample and supported 79%–105% of the reference slab's ultimate load. The concrete slab's shear strength depends on its effective mass. Bubbled deck slabs have lower shear resistance than SS slabs due to the plastic bubbles. According to theoretical estimates, the voided slab has 60–80% of the shear strength of an SS of the same depth. Therefore, all bubbled deck slabs' shear capacity must be reduced by 0.6. Further testing by authors in [32] disclosed that many CFRP layers on slabs increased external force resistance. Deflection is inversely related to coating count. Many studies and experiments have explored the effectiveness of GFRP rebars in strengthening beams and concrete slabs. Authors in [12] examined how lightweight concrete and GFRP composite bars increase bridge deck slab durability and toughness. Many technological, material and architectural solutions have been developed to extend bridge deck slab life. Since lightweight concrete reduces bridge construction weight, these materials can lower bridge costs over time. Slabs reinforced with FRP bars have been extensively studied. Authors in [33] tested 12 one-way RC slabs reinforced with BFRP and GFRP bars for flexural behavior under four-point loading. All slab strips showed steep linear elastic behavior until the first crack, regardless of the FRP bar type. Seven BFRP-reinforced one-way slabs were tested in [34]. They tested three reinforcement types with 6, 10, and 12 mm diameters. Linear failure was observed in Basalt Fiber-Reinforced Polymer (BFRP)-reinforced slabs, according to the experimental findings, indicating that the occurrence results when the concrete attains its maximum strength and fractures. Authors in [35] examined

employing FRP instead of steel reinforcement in locations prone to severe weather and magnetic fields. This study analyzed seven slabs. One slab had steel reinforcement, whereas the others had GFRP rebars. Slabs were two-point bending. Reinforcement ratio and shear span to effective depth ratios were significant experimental parameters. The study found that all GFRP-reinforced slabs were bilinear elastic until failure and deflection decreased with increasing reinforcement ratio. One-way bubbled concrete slabs transmit force differently than two-way slabs. These forces are only transmitted longitudinally. Therefore, any weakness in this direction generates slab collapse early. Moreover, voids in this direction may cause surface challenges. Few works have considered one-way voided slabs. This study highlights the presence of voids and GFRP reinforcement combined together. It shows how they affect one-way concrete BS' ultimate load, deformation, and stiffness, comparing them to the reference SS. On the other hand, this study examines how steel I-section internal strengthening improves BS' ultimate load capacity, stiffness, deformations, and shear resistance.

II. EXPERIMENTAL WORK

A. Tested Specimens

Six structural concrete slabs (2600 mm long, 600 mm wide, 150 mm deep) were tested under two-point bending. Using a hydraulic jack, the slabs received two symmetrical concentrated loads ($a/d=6.4$). Table I depicts the six slabs arranged into two groups: one with two un-strengthened reference SS and BS (SS1 and BS1), respectively, and the other with four internally strengthened BS with I-shaped steel beams. The first specimen in this group (BS1-2I) had two steel I-shaped beams in cross-section with dimensions of 72×30×6 mm, fixed between ball lines without CSC. The second specimen (BS1-4I), had four I-shaped steel beams in cross-section dimensions of 50×25 mm, with flange and web thicknesses of 5 mm and 3 mm, respectively, without CSC, having an equivalent cross-sectional area of the steel I-shaped beams in BS1-2I specimen. The other specimens (BS1-2I-SC and BS1-4I-SC) had CSC in dimensions of 30×30×3 mm and 15×30×3 mm, fixed on the top surface of the sections in specimen BS1-2I-SC and BS1-4I-SC, respectively, Figure 1 provides the details of steel I-sections. Each specimen contained 95 polymer sphere voids of 90 mm diameter with a self-weight reduction of 15.48% whereas the ratio of the diameter of a sphere to the depth of the slab (D/H) was 0.6. Five pieces of steel bent-up bars (310 mm long) were placed near the supports at $d/2$ distance.

B. Material Properties

SCC with 45.43 MPa cylinder compressive strength was used to make the slabs. Six 150×150×150 mm standard cubes and six 150×300 mm standard cylinders were deployed to determine the average concrete compressive strength. Tables II and III list SCC and voided/SS materials.

C. Specimen Details

Deformed GFRP reinforcing meshes were attached to the slab's upper and lower surfaces during testing. Ten longitudinal and 38 transverse 10 mm bars were on each mesh. Following

ACI 440.1R-15 guidance, the over-reinforcement ratio $\rho_f = A_f / bd$ was employed to provide compression control, where $\rho_f = 0.0104$, $A_f =$ GFRP reinforcing bar area, $b =$ slab width, and d is the effective depth [36]. Five BS and one SS were cast to

investigate how the parameters affected the behavior of the control and strengthened the former. Each BS has 115 mm longitudinal and transverse bubble spacing. See Figure 2 and Table IV for slab specimen details.

TABLE I. DESIGNATION OF THE EXPERIMENTAL SLABS

Group	Slab designation	Characteristic	Dimensions of steel I-shaped beams	Shear reinforcement (bent-up bar)
Group one	SS1	SS (control)	---	---
	BS1	BS (control)	---	---
Group two	BS1-2I	BS with 2 steel I-shaped beams, without CSC.	72×30×6 mm	5 PCS. $\Phi 10$ on each side near support (310 mm in length)
	BS1-4I	BS with 4 steel I-shaped beams having an equivalent cross-sectional area of 2 I-shaped beams, without CSC.	50×25 mm Flange thick. = 5 mm Web thick. = 3 mm	5 PCS. $\Phi 10$ on each side near support (310 mm in length)
	BS1-2I-SC	BS with 2 steel I-shaped beams, with CSC.	72×30×6 mm	5 PCS. $\Phi 10$ on each side near support (310 mm in length)
	BS1-4I-SC	BS with 4 steel I-shaped beams having an equivalent cross-sectional area of 2 I-shaped beams, with CSC.	50×25 mm Flange thick. = 5 mm Web thick. = 3 mm	5 PCS. $\Phi 10$ on each side near support (310 mm in length)

TABLE II. MATERIALS PROPERTIES OF SELF-COMPACTING CONCRETE

Material	Property
Cement	Ordinary Portland Cement (OPC) Type I
Sand	Natural fine aggregate of 4.75 mm maximum size
Gravel	Crushed coarse aggregate of 10 mm maximum size
Micro silica	Silica fume from Sika Company, comprising around 8% of the cement's weight, to create self-compacting concrete specimens
Limestone powder	Limestone powder particles with size less than 0.125 mm according to EFNARC (2005)
Super-plasticizer	Third-generation superplasticizer concrete admixture Sika ViscoCrete-5930. The product conforms to ASTM-C-494 type F.
Water	Ordinary tap water

TABLE III. MATERIAL PROPERTIES OF BUBBLED AND SOLID SLABS

Material	Property
GFRP bars	Deformed GFRP bars of 10 mm diameter having a tensile strength at break of 1207 MPa, elongation 2.5%, and modulus of elasticity of 48000 MPa
Steel I-sections	Built-up steel I-shaped beams were made by welding flat bars together, having 454.8 MPa of yield strength and 575.7 MPa of ultimate strength, which falls within the range of Grade 60, elongation 17.33%, and modulus of elasticity equal to 259000 MPa
Bent-up steel bars	According to ASTM-A615/A615M-20, deformed steel bars of 10 mm diameter having a yield strength of 567 MPa, ultimate strength of 717.8 MPa, and modulus of elasticity of 220000 MPa, which falls within the range of Grade 60
CSC	CSC was made by cutting and crooking flat bars, same as the steel I-sections
Balls	The plastic spheres utilized comprised 90 mm-diameter HDPE molds.

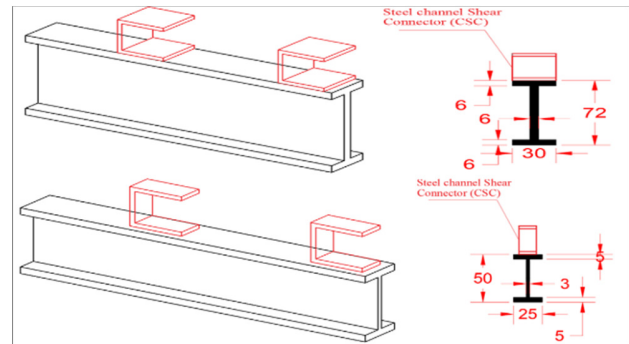


Fig. 1. Details of steel I-shaped beams.

D. Preparation of Bubbled Slabs

Transverse GFRP bars were spaced accordingly to accommodate ball diameter and center distance. To prevent horizontal displacement, the balls were aligned with the square centers of the reinforcement mesh in the tension zone (95 balls with a diameter of 90 mm were used in each BS specimen, resulting in a 15.48% self-weight reduction). Ball diameter and center distance were taken into account. The reinforcement mesh is placed on the wooden mold and lifted to the required concrete cover with 20 mm plastic spacers. By bolting the bottom reinforcement mesh to the wooden mold and adding tiny curved steel pieces, the mesh cannot move and provides 25 mm side concrete cover. Flat bars are welded together to form an I-shaped steel beam. Special machines cut and bend flat bars to manufacture CSC with the needed size. Installing the CSC parts requires welding them to an I-shaped steel surface with a 90 mm spacing. The steel I-shape, including the CSC, is placed between the longitudinal rows of balls and is connected to the reinforcement mesh. The compression zone's top reinforcement mesh is placed above the balls to prevent vertical movement. The top and bottom reinforcement meshes are connected by plastic zip ties.

TABLE IV. DETAILS OF THE TESTED SPECIMENS

G	Specimen designation	Specimen thickness (mm)	Diameter of a sphere (mm)	Number of spheres	D/H	Reduction in self-weight ratio (%)	Distance between spheres c/c, (mm)	Type of internal strengthening
1	SS1	150	---	---	---	---	---	Un-strengthening
	BS1		90	95	0.6	15.48	115	Un-strengthening
2	BS1-2I	150	90	95	0.6	15.48	115	Steel 2I-shaped, without CSC
	BS1-4I							Steel 4I-shaped, without CSC
	BS1-2I-SC							Steel 2I-shaped, with CSC
	BS1-4I-SC							Steel 4I-shaped, with CSC

Figures 3 and 4 portray a bent-up steel bar (10 mm diameter) with a 310 mm length inserted between the two reinforcing meshes in five pieces along the specimen's transverse direction near the supports to withstand shear stress. All slabs were tested under two-point bending until full failure ($a/d=6.4$, shear span ratio a to effective depth d).

point bending and the load was applied with a 2 kN increment until failure. Figure 5 displays the testing setup and equipment. Each slab met ACI 440.1R-15 criteria [36]. Slab deflections and cracking formation were measured at each load level.

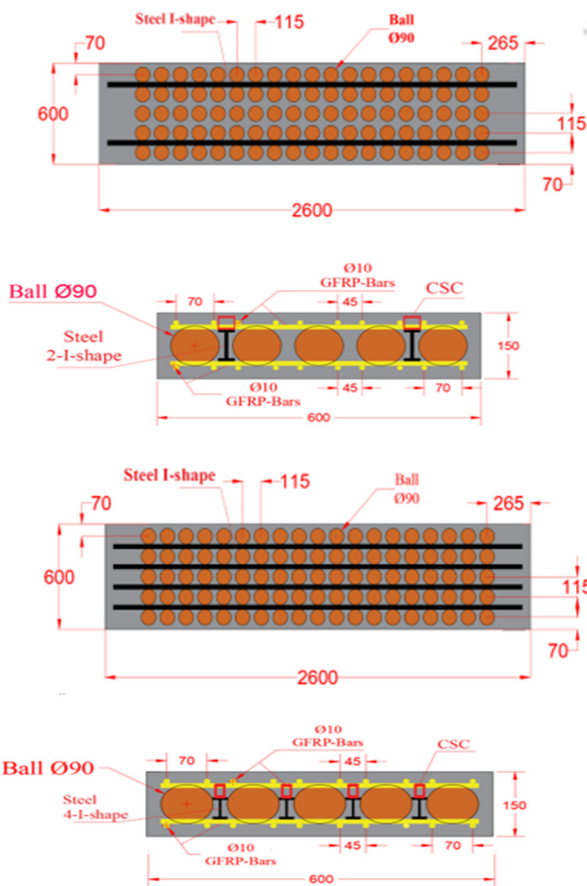


Fig. 2. Distribution of reinforcement and bubbles in specimen BS1-2I-SC and BS1-4I-SC.

E. Test Instrumentation and Measurements

1) Load Measurements

The slabs were painted white to make cracking formation easier to be seen during testing. In this test, the slabs were supported by two 2400 mm steel beams. Every slab specimen was tested after 28 days. Each slab was tested with a 500 kN hydraulic jack until it failed. Slabs were supported under two-



Fig. 3. Pictures of the construction of the test slabs.

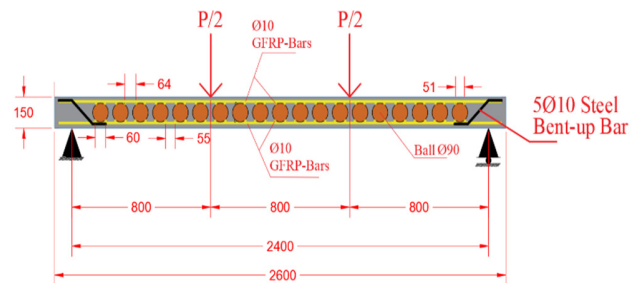


Fig. 4. Longitudinal cross-section in BS including steel bent-up bar.

2) Deflection Measurement

The deflection was measured using two Linear Variable Differential Transducers (LVDTs) and one dial gauge. Midpoint slabs held the LVDTs and the dial gauge, and a steel frame (Figure 6), held the LVDTs and the dial gauges.

3) GFRP Strain Measurement

Figure 7 illustrates two strain gauges of 5 mm length that were attached to the bottom GFRP mesh at its center. The wires of the LVDTs were connected to a data recorder. Using specialized computer software enabled the recording of four readings per second for the strain gauge and LVDT. Several readings were ultimately obtained for each measurement. Statistical analysis methods were utilized to interpret and assess the outcomes.

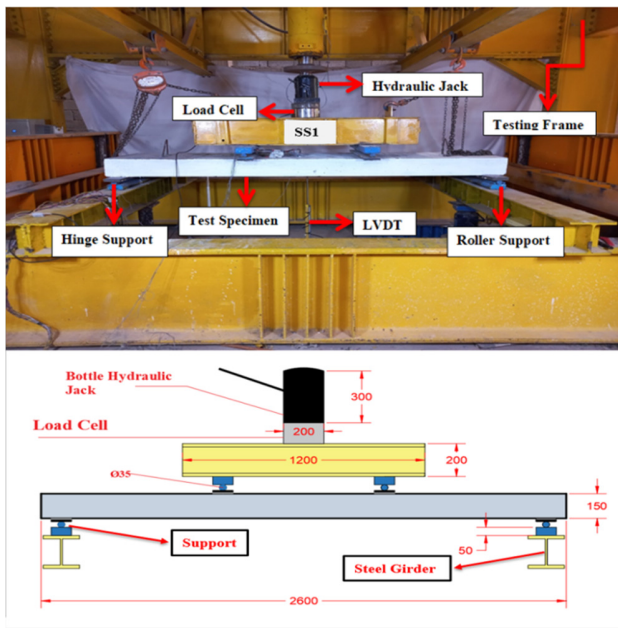


Fig. 5. Test specimen setup.



Fig. 6. LVDT and dial gauge test setup.

4) Steel Strain Measurement

Two strain gauges with a gauge length of 5 mm were affixed to each specimen, including the I-shaped structures (2I-shaped and 4I-shaped) to quantify the strain in the steel. Each strain gauge was placed at the midpoint of the upper fiber of the steel I-shaped beams, as observed in Figure 7.

5) Concrete Strain Measurement

Two strain gauges measuring 60 mm in length were attached to the concrete compressive area on each slab specimen. As manifested in Figure 7, these instruments were positioned at the midpoint of the upper surface of the slabs.

III. RESULTS AND DISCUSSION

This study compares conventional and strengthened BS. Table V shows all the parameters needed to compare SS and BS and understand their behaviors. Key parameters include first crack load (P_{cr}), mid-span deflection at the first crack (Δ_{cr}), deflection at 0.7 times the ultimate strength of SS1, slab ultimate strength (P_u), ultimate deflection (Δ_u), and failure type and mode.

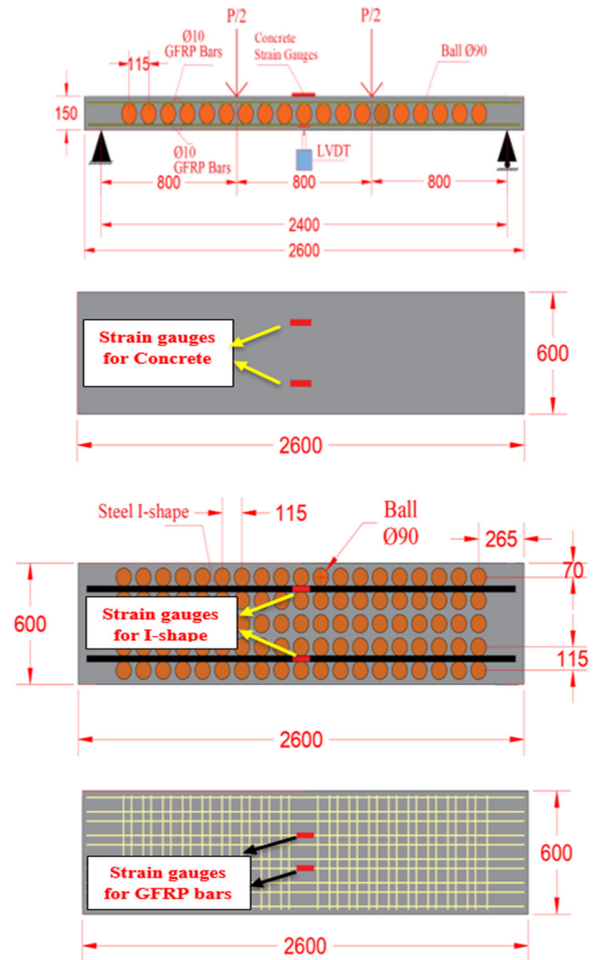


Fig. 7. Strain gauge locations.

A. Load-Deflection Response

Table V demonstrates the flexural failure in three strengthened slabs, and shear failure in two un-strengthened reference slabs and one strengthened slab. Figure 8 portrays load mid-span versus deflection. The initial loading did not cause cracking, resulting in linear load-deflection behavior. For this, concrete and GFRP bars experienced linear elastic deformation. Flexural stiffness decreases with cracking, while cracks increase as the load increases, reducing these slabs' stiffness. BS1 deflected more due to its flexibility, with plastic balls in the matrix reducing stiffness and increasing deflection. Group one slab (SS1) is stiffer than BS1. Flexural part deflection is usually controlled by service load, which accounts for 70% of the SS1's ultimate load. Thus, $P_s = 206.53$ kN. The control BS1 deflected 68.95 mm under the load, 27% more than SS1. Internally strengthened BS performed better than un-strengthened slabs, as internal strengthening with steel I-shaped beams increased stiffness above the SS1. These steel beams increased the specimen's moment of inertia, thus decreasing deflection. The BS specimens, BS1-2I and BS1-2I-SC, had 10% and 11% higher stiffness than SS1 and 20% and 21% higher stiffness than BS1, respectively. BS1-4I and BS1-4I-SC were 10% and 11% stiffer than SS1 and 20% and 21% stiffer

than BS1, respectively. It was shown that BS1-4I-SC has the same stiffness as BS1-2I-SC. At service load, strengthened BS deflected less than SS1 and BS1. In particular, specimens BS1-2I and BS1-2I-SC had deflections of 38% and 53%, and BS1-4I and BS1-4I-SC had deflections of 41% and 49%, lower than SS1, respectively. They also achieved 55%, 63% and 54%, and 60% smaller deflections than BS1 specimens, respectively.

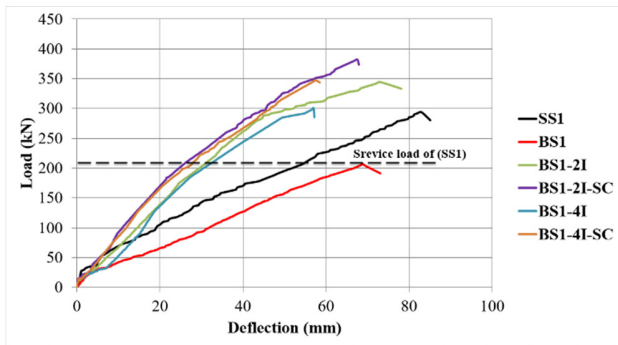


Fig. 8. Load VS. mid-span deflection of all tested specimens.

B. Crack Pattern and Failure Mode

1) General Behavior of Conventional Bubbled and Solid Deck Slab

The pure bending zone has the maximum bending moment, hence the first flexural crack occurs there. Flexural shear cracks developed outside the pure bending zone, and certain flexural cracks expanded in width and height until failure for all specimens. Interaction between polymer spheres that produce voids in BS and cracks reduces cracks and increases crack width, allowing rapid propagation from solid to void zone. Tensile stresses, which were greater than the concrete modulus of rupture, caused flexural cracks in concrete slab soffits. Flexural cracks parallel to these propagate across the slab's thickness. Deflections at the slab mid-span increased with load. Figure 9 illustrates flexural-shear cracks as the slab collapses. In un-strengthened slabs (SS1 and BS1), flexural-shear cracks are formed after flexural cracking, causing shear failure. The tension face of SS1 and BS1 exhibited vertical flexural cracking. A significant combination of both shear and flexural stresses at the head of a flexural cracking causes a shear failure mode with concrete crushing near the point load, displayed in Figure 9. With increasing load, the crack propagates higher, crushing the SS and BS. Bubbled specimens were crushed at levels lower than those of the reference SS, as expected. Due to the massive concrete removal from the voids, their moment of inertia decreased instantly. In the first group of the test

subjects, the control models', SS1 and BS1, shear failure crushed the concrete near the point load. Figure 9 shows SS and BS break brittle, resulting in concrete collapse. The failure mode and crack pattern of each specimen are displayed in Figure 9.

2) General Behavior of Strengthened Bubbled Deck Slab

The study reveals that internal strengthening with steel I-shaped beams significantly improved the overall strength and shear resistance of BS in the second group. The strengthening process was implemented in two forms: two I-shaped specimens (BS1-2I and BS1-2I-SC) with/without CSC, and four I-shaped specimens (BS1-4I and BS1-4I-SC), with/without CSC. The results exhibited significant improvements in deflection, ultimate strength, stiffness, and crack pattern. The second group had a noticeable and substantial effect due to the greater moment of inertia demonstrated by these specimens compared to SS1 and BS1. Crack propagation occurred as the load increased, with certain cracks extending into the compression zone for both BS1-2I-SC and BS1-4I-SC. The strengthened concrete slabs developed cracks under greater load than SS1 and BS1, causing the mode of failure to transfer in the direction of the compression zone. The second group of strengthened BS experienced flexural failure within the compression (BS1-4I).

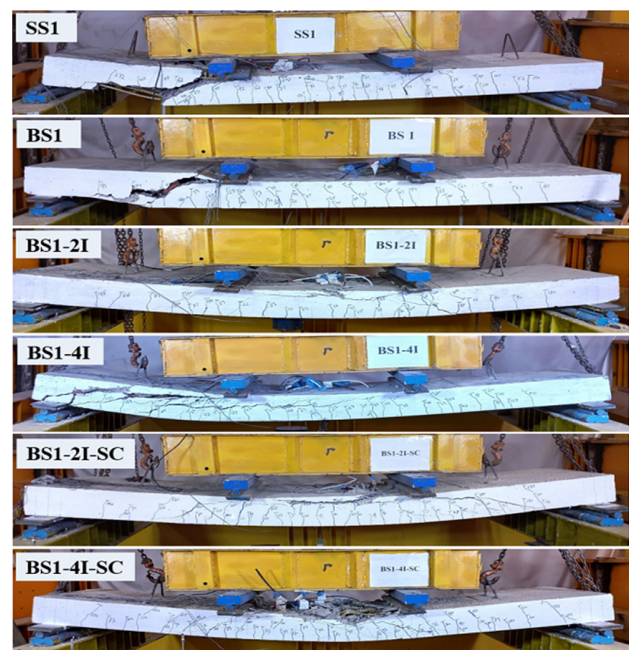


Fig. 9. Cracks pattern and failure mode for each investigated specimen.

TABLE V. LOAD AND DEFLECTION COMPARISON FOR ALL TESTED SPECIMENS

Slab designation	P_{cr} (KN)	Δ_{cr} (mm)	Δ at 0.7 P_u of SS1 (mm)	P_u (KN)	Δ_u (mm)	Type of failure	Failure mode
SS1	37	4.7	54.27	293.59	83	Shear	Brittle (concrete-crushing)
BS1	25	3.46	68.95	206.53	68.95	Shear	Brittle (concrete-crushing)
BS1-2I	23	2.65	30.7	344.48	73.04	Flexural compression	Brittle (concrete-crushing)
BS1-4I	22	2.54	31.85	300.92	56.94	Shear	Brittle (concrete-crushing)
BS1-2I-SC	25	2.85	25.67	382.35	67.57	Flexural compression	Brittle (concrete-crushing)
BS1-4I-SC	32	3.65	27.64	347.15	57.47	Flexural compression	Brittle (concrete-crushing)

These failures resulted from concrete crushing on the upper surface of the specimen in the pure bending region between the loads, caused by flexural failure, and one failure outside the pure bending region for the specimen BS1-4I caused by shear failure. The observed failure mode can be categorized as brittle, as evidenced by the concrete's recorded strains as it approached its maximal strain.

C. Ultimate Load Capacity

Figure 8 and Table V show the maximal load attained by slab specimens, with the strengthened bubbled slab (BS1-2I-SC) demonstrating the greatest failure load. The ultimate load capacity of BS1-2I-SC and BS1-4I-SC was enhanced by 30% and 18%, respectively, compared to SS1, whereas the capacity increased by 85% and 68% compared to BS1. Furthermore, in comparison to the specimen SS1, slab specimens BS1-2I and BS1-4I increased ultimate load by approximately 17% and 2%, and by 67% and 46% when compared to BS1, respectively. The BS1's ultimate load capacity significantly decreased by 30% compared to the SS1, attributed to the presence of voids within the specimen, which reduced the moment of inertia and stiffness.

D. Load-Strain Curves

1) Concrete Strain

The study analyzed the compressive behavior of concrete specimens using two strain gauges placed on their upper surfaces, while the average readings were taken into consideration. The strain gauge readings were nearly negligible before cracks appeared and the concrete was crushed, but increased with higher applied loads until collapse, as seen in Figure 10.

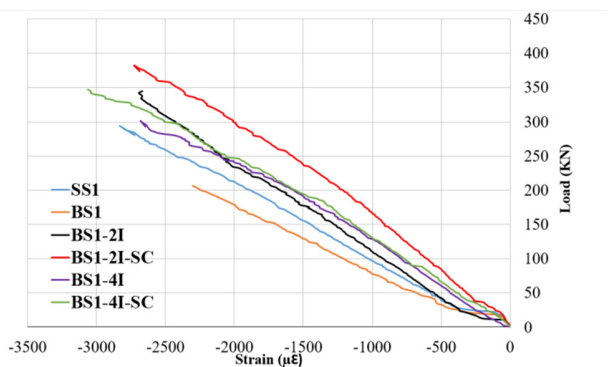


Fig. 10. Load-compressive strain curves of concrete of all tested specimens.

The service load of the solid slab SS1 (206.53 kN) was used for comparison. The un-strengthened bubbled slab (BS1) had the highest strain, with 18% more strain than SS1, at the same load level. Balls and their reduction in concrete reduced the specimen's BS1 stiffness compared to SS1. The strengthened bubbled slabs BS1-2I-SC, BS1-4I-SC, BS1-2I, and BS1-4I had lower strain than the un-strengthened slab (BS1) by 45%, 30%, 25%, and 29%, respectively. They also exhibited reduced strain by 35%, 17%, 11%, and 16% compared to SS1, respectively. The steel I-shaped beams added moment of inertia to the specimens, increasing their stiffness.

The strengthened bubbled slabs had less deflection and were less flexible. Table VI shows the strain values of all specimens at the ultimate and service stages under similar loading circumstances of 0.7 times the P_u of SS1.

2) GFRP Strain

Figure 11 displays the load-strain curve of GFRP-bar longitudinal reinforcement at the bottom mid-span. The average readings of two tensile strains were taken. The GFRP reinforcement has a bilinear load-strain relationship, similar to that of the slab load-deflection. The first group specimens' bottom reinforcement strains were measured and compared to the second group specimens' strain response at the same loading stage (0.7 times that of SS1). The un-strengthened BS model (BS1) had larger strains than the others. The strengthened BS specimens exhibited significantly reduced strain, due to the steel I-shaped strengthening slabs. The un-strengthened BS1 had 21% more strain than that of the SS1. SS1 strain is 168%, 118%, 200%, and 204% larger than that of the strengthened BS (BS1-2I-SC, BS1-2I, BS1-4I-SC, and BS1-4I, respectively). The BS1 strains were 224%, 164%, 264%, and 268% more than those of BS1-2I-SC, BS1-2I, BS1-4I-SC, and BS1-4I, respectively. Continuous loading until the strengthened slab broke indicated maximum deformation. Table VI presents the specimen strain values for concrete and GFRP bars at ultimate and service loading stages. Figure 11 shows that GFRP bars did not rupture during loading, suggesting that their ultimate strain did not reach its maximum. Table V manifests the failure types and modes for the first and second groups.

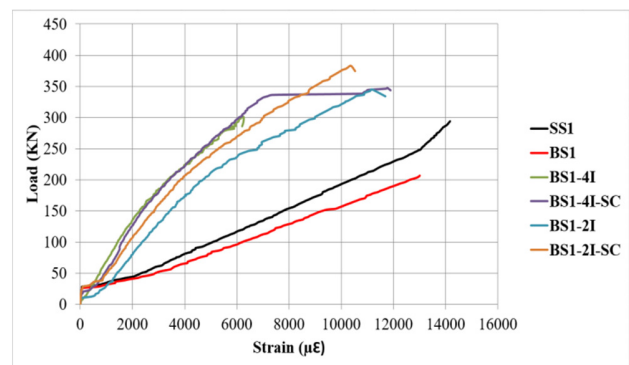


Fig. 11. Load-strain curves of bottom GFRP-bars.

TABLE VI. STRAIN OF GFRP AND CONCRETE AT THE SERVICE AND ULTIMATE LOADING STAGE

Slab designation	Ultimate load P_u (KN)	Avg. strain at the service loading stage (0.7 P_u of SS1)		Avg. strain at the ultimate loading stage ($\mu\epsilon$)	
		GFRP-bar ($\mu\epsilon$)	Concrete ($\mu\epsilon$)	GFRP-bar ($\mu\epsilon$)	Concrete ($\mu\epsilon$)
SS1	293.59	10751.28	1949.90	14169.29	2829.67
BS1	206.53	13015.30	2301.60	13015.30	2301.60
BS1-2I	344.48	4923.96	1735	11181.27	2667.52
BS1-4I	300.92	3540.82	1640.04	6249.61	2679.92
BS1-2I-SC	382.35	4017.47	1258.14	10379.41	2726.06
BS1-4I-SC	347.15	3578.41	1615.74	11774.96	3064.42

3) Steel I-Shape Specimen Strain

Figure 12 depicts the average load-strain curves as a function of applied loads for specimens with steel I-shaped beams. Each strengthened specimen has two strain gauges on the implanted steel I-shaped beams on the top flange at mid-spans, as observed in Figure 7. Each specimen's average was taken. BS1-2I-SC and BS1-2I composite specimens had ultimate tensile strains of 1150.73 and 1683.38 micro-strains at 382.35 kN and 344.48 kN, respectively, whereas the strengthened specimens BS1-4I-SC and BS1-4I exhibited 1510.98 and 1140.27 micro-strains at 347.15 kN and 300.92 kN, respectively. BS1-2I-SC specimens showed 37% less strain than BS1-4I-SC due to their lower top surface of the Neutral Axis (NA). The specimen operated more in the tension zone than the steel I-section top surface (BS1-2I-SC), which is closer to the NA. BS1-2I achieved 1683.38 strain but did not yield or plasticize, which is proven by comparing specimen strain to laboratory strain for steel I-shaped specimens.

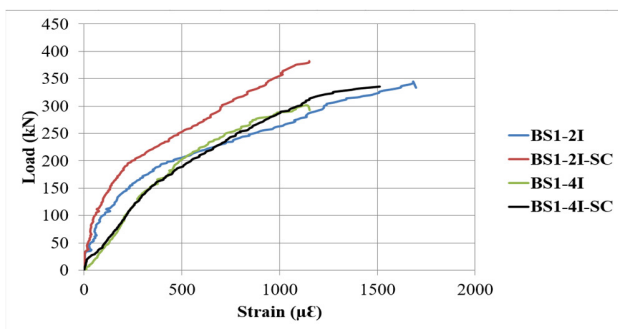


Fig. 12. Load-strain curves of top flange surface of specimens with steel I-shaped beams.

E. Flexural Stiffness of Slabs

Flexural stiffness refers to a slab's resistance to bending, influenced by factors like elasticity modulus, effective length, moment of inertia, and boundary conditions. The secant stiffness of slabs is determined by their load-deflection slope, which measures their flexural stiffness. Cracks and low concrete-reinforcement bar bonding reduce a slab's rigidity after loading. Figure 13 demonstrates that all K_u values are lower than K_{cr} . Voids in the slab and flexural rigidity reduction can lead to decreased stiffness during ultimate loading and cracking [37]. To determine secant stiffness, (1) and (2) were applied:

$$K_{cr} = \frac{P_{cr}}{\Delta_{cr}} \tag{1}$$

$$K_u = \frac{P_u}{\Delta_u} \tag{2}$$

Table VII demonstrates the stiffness of specimens during cracking (K_{cr}) and ultimate (K_u) stages, with secant stiffness (K) varying between the two phases. BS1 had 8% and 15% lower flexural stiffness during cracking and ultimate loading phases, respectively, than SS1, due to the reduced concrete content, reducing the BS' moment of inertia and model stiffness. Internally strengthening BS with steel I-sections increases stiffness, which in turn increases the slab's inertia.

Compared to BS1, the second group of strengthened BS models BS1-2I-SC, BS1-2I, BS1-4I-SC, and BS1-4I had 21%, 20%, 21%, and 20% higher stiffness at the cracking loading stage, respectively. These models had superior stiffness at the ultimate loading stage by 88%, 58%, 102%, and 78% over BS1. In contrast, the second group's models gained stiffness by 11%, 10%, 11%, and 10% during cracking loading, and in the ultimate loading step, had 60%, 33%, 71%, and 50% higher stiffness than SS1, respectively.

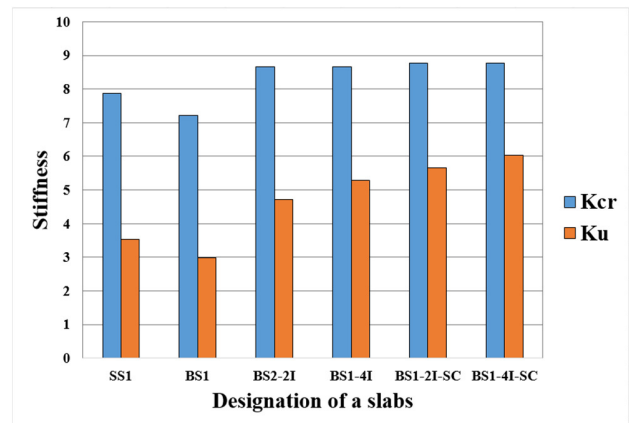


Fig. 13. Stiffness of all tested specimens at cracking and ultimate stage.

TABLE VII. STIFFNESS AT CRACKING AND ULTIMATE STAGE

Specimen	Cracking stage			Ultimate stage		
	P_{cr} (KN)	Δ_{cr} (mm)	K_{cr} (KN/mm)	P_u (KN)	Δ_u (mm)	K_u (KN/mm)
SS1	37	4.7	7.87	293.59	83	3.53
BS1	25	3.46	7.22	206.53	68.95	2.99
BS1-2I	23	2.65	8.67	344.48	73.04	4.71
BS1-4I	22	2.54	8.66	300.92	56.94	5.28
BS1-2I-SC	25	2.85	8.77	382.35	67.57	5.65
BS1-4I-SC	32	3.65	8.76	347.15	57.47	6.04

IV. BRITISH REGULATIONS LIMITS FOR BS

This section will discuss some significant limitations associated with BS, including shear strength, flexural stiffness, and rigidity factor when compared to SS. Research and experiments demonstrated that BS specimens have a flexural stiffness of 87% compared to that of SS. This results in an increase in deflection during the Service Loading Stage (SLS). Given that the shear forces are high near the supports, to ensure shear resistance, it is advisable to keep the region surrounding the columns or supports solid, as concrete directly affects shear resistance. When designing, a shear resistance value of 60% of SS is considered. Conversely, the UK regulations specify that the stiffness factor for BS should be set at 0.88 for SS. Table VIII presents a comparison of the experimental findings from this work with the required limits for BS according to the British standards. It is important to note that the values specified in the British standards are specifically for BS reinforced with steel bars.

TABLE VIII. COMPARISON BETWEEN UK LIMITATIONS FOR BS WITH THE EXPERIMENTAL RESULTS

In % of solid slabs	UK standards for BS reinforced with steel bars	Experimental results of BS reinforced with GFRP bars	Notes
Flexural stiffness	87%	85%	The reason for this difference is that GFRP has less stiffness than steel
Shear resistance	60%	66%	---
Rigidity ractor	0.88	0.98	---

V. ADVANTAGES AND DISADVANTAGES OF EMBEDDED STEEL I-SECTIONS

The comparison results are depicted in Table IX.

TABLE IX. COMPARISON OF ADVANTAGES AND DISADVANTAGES OF EMBEDDED STEEL I-SHAPES IN BS

Advantages	Disadvantages
The use of embedded steel I-shaped sections with BS reinforced by GFRP bars does not increase self-weight, as GFRP's weight is four times less than that of steel's, and does not affect the weight reduction achieved by the BS.	The use of steel I-sections in BS reinforced by steel bars increases slab self-weight, which reduces the amount of weight reduction of the BS
The use of I-sections enhances the strength of the BS reinforced with GFRP bars while maintaining the slab's weight reduction ratio	It needs paint to protect it against environmental influences.
Embedded steel I-sections in BS increase flexural stiffnes.	---

VI. CONCLUSION

This study investigated the flexural behavior of one-way concrete Bubbled Slabs (BS) reinforced with Glass Fiber-Reinforced Polymer (GFRP) rebars and steel I-shaped beams. Static two-point bending was applied to assess the structural integrity of the specimens. Cracking resistance, deflection in response to applied stresses, ultimate strength, and failure mode were assessed. The subsequent conclusions are derived from the experiments conducted in this study:

- The slabs subjected to testing and reinforced with GFRP bars demonstrate bilinear behavior until they approach the point of failure.
- After cracks formed at its ultimate phase, the un-strengthened BS had 15% less stiffness than Solid Slab (SS) due to its decreased moment of inertia. However, strengthened BS specimens with two and four steel I-sections with/without Channel Shear Connectors' (CSC) had 88%, 102%, 58%, and 78% higher stiffness than un-strengthened BS, respectively, and 60%, 71%, 33%, and 50% higher stiffness than SS, respectively.
- Un-strengthened BS had 15% less ultimate strength than SS. However, enhanced BS with two and four steel I-sections with/without CSC exhibited increased ultimate strength by 85%, 68%, 67%, and 46% compared to the un-

strengthened BS, respectively, and 30%, 18%, 17%, and 2%, compared to the SS, respectively.

- The presence of GFRP rebars and plastic spherical voids increased the width of cracks and reduced their number. Conversely, the strengthening of BS significantly reduced the quantity and width of maximum cracks.
- Implementing internal strengthening in the form of steel I-shaped sections averted service cracks in BS. Additionally, shear strength, first cracking stress, flexural strength, and load-bearing capacity were enhanced.
- The deflection of the strengthened BS comprising two and four steel I-sections with/without CSC was 53%, 49%, 43%, and 41% less than that of the SS, respectively. Furthermore, the deflection exhibited a reduction of 63%, 60%, 56%, and 54% in comparison to the un-strengthened BS.
- Brittle shear failure caused concrete crushing near the point load in the un-strengthened slabs of the test subjects. Strengthened BS experienced flexural failure in the compression zone, with the mode of failure being considered "brittle". However, the inclusion of steel I-shaped beams as internal strengthening altered the type of failure from shear to compression.
- Un-strengthened BS have 66% of the shear strength of SS. Furthermore, the inclusion of steel I-sections in BS (specifically, two and four I-sections with CSC) significantly increased the shear strength by approximately 12 and 10 times, compared to SS, respectively, and by 18 and 15 times, compared to un-strengthened BS, respectively.
- Strengthened BS exhibited reduced concrete-compressive strain by 45% and 30% for models with two and four steel I-shaped sections with CSC, compared to the un-strengthened BS specimen, respectively.
- The first significant accomplishment of the study was the participants' self-weight reduction through the attainment of an acceptable ultimate strength by placing plastic spheres into slabs. Furthermore, internal strengthening with steel I-shaped beams enhanced the BS' deflection, stiffness, fracture resistance, carrying capacity, flexural strength, and shear strength.

According to this study results, I-shaped steel is recommended to strengthen BS and other structural components internally. The sections' moment of inertia increases ultimate load capacity, decreases deflection and cracking, and improves slab stiffness.

ACKNOWLEDGMENT

The authors express their gratitude to the structural lab and engineering consulting bureau at Baghdad University/College of Engineering for their support in conducting experimental tests on concrete slab samples and investigating the materials used in the study, as well as the Department of Civil Engineering for their technical assistance.

REFERENCES

- [1] B. G. Bhade and S. M. Barelikar, "An Experimental Study on Two Way Bubble Deck Slab with Spherical Hollow Balls," *International Journal of Recent Scientific Research*, vol. 7, no. 6, pp. 11621-11626, June, 2016.
- [2] N. Oukaili and H. Yaseen, "Effect of prestressing force on performance of polymer bubbled deck slabs," in *The 7th International Conference on FRP Composites in Civil Engineering*, Vancouver, BC, Canada, Aug. 2014, pp. 1-6.
- [3] C. Marais, "Design Adjustment Factors and the Economical Applications of Concrete Flat-Slabs with Internal Spherical Voids in South Africa," M.S. thesis, University of Pretoria, Pretoria, South Africa, 2009.
- [4] N. Oukaili and H. H. Yasseen, "Experimental Investigations on the Strength and Serviceability of Biaxial Hollow Concrete Slabs," *Journal of Engineering*, vol. 22, no. 11, pp. 36-54, Nov. 2016, <https://doi.org/10.31026/j.eng.2016.11.03>.
- [5] N. Oukaili, H. Merie, A. Allawi, and G. Wardeh, "Reduced Volume Approach to Evaluate Biaxial Bubbled Slabs' Resistance to Punching Shear," *Buildings*, vol. 14, no. 3, Mar. 2024, Art. no. 676, <https://doi.org/10.3390/buildings14030676>.
- [6] D. H. Al-Rashedi and A. H. A. Al-Ahmed, "Two-Way Bubbled Slabs Strengthened by Prestressing Strands," *IOP Conference Series: Materials Science and Engineering*, vol. 901, no. 1, Dec. 2020, Art. no. 012011, <https://doi.org/10.1088/1757-899X/901/1/012011>.
- [7] T. Lai, "Structural behavior of BubbleDeck® slabs and their application to lightweight bridge decks," M.S. thesis, Massachusetts Institute of Technology, Cambridge, MA, USA, 2010.
- [8] S. Calin and C. Asavaoie, "Method for bubble deck concrete slab with gaps," *Buletinul Institutului Politehnic din Iasi*, vol. 55, no. 2, pp. 63-70, 2009.
- [9] V. Abishek and G. R. Iyappan, "Study on Flexural Behavior of Bubble Deck Slab Strengthened with FRP," *Journal of Physics: Conference Series*, vol. 2040, no. 1, Jul. 2021, Art. no. 012018, <https://doi.org/10.1088/1742-6596/2040/1/012018>.
- [10] A. S. Mahdi and S. D. Mohammed, "Experimental and Numerical Analysis of Bubbles Distribution Influence in BubbleDeck Slab under Harmonic Load Effect," *Engineering, Technology & Applied Science Research*, vol. 11, no. 1, pp. 6645-6649, Feb. 2021, <https://doi.org/10.48084/etasr.3963>.
- [11] M. Abas Golham and A. H. A. Al-Ahmed, "Behavior of GFRP reinforced concrete slabs with openings strengthened by CFRP strips," *Results in Engineering*, vol. 18, Jun. 2023, Art. no. 101033, <https://doi.org/10.1016/j.rineng.2023.101033>.
- [12] A. Wiater and T. Siwowski, "Serviceability and ultimate behaviour of GFRP reinforced lightweight concrete slabs: Experimental test versus code prediction," *Composite Structures*, vol. 239, May 2020, Art. no. 112020, <https://doi.org/10.1016/j.compstruct.2020.112020>.
- [13] Y. Zheng, C. Li, and G. Yu, "Investigation of structural behaviours of laterally restrained GFRP reinforced concrete slabs," *Composites Part B: Engineering*, vol. 43, no. 3, pp. 1586-1597, Apr. 2012, <https://doi.org/10.1016/j.compositesb.2011.11.012>.
- [14] A. Veljkovic, V. Carvelli, and M. Rezazadeh, "Modelling the bond in GFRP bar reinforced concrete thin structural members," *Structures*, vol. 24, pp. 13-26, Apr. 2020, <https://doi.org/10.1016/j.istruc.2019.12.027>.
- [15] M. A. Issa, A. A. Allawi, and N. Oukaili, "Effects of GFRP Stirrup Spacing on the Behavior of Doubly GFRP-Reinforced Concrete Beams," *Civil Engineering Journal*, vol. 10, no. 2, pp. 502-520, Feb. 2024, <https://doi.org/10.28991/CEJ-2024-010-02-011>.
- [16] M. A. Golham and A. H. A. Al-Ahmed, "Strengthening of GFRP Reinforced Concrete Slabs with Openings," *Journal of Engineering*, vol. 30, no. 1, pp. 157-172, Jan. 2024, <https://doi.org/10.31026/j.eng.2024.01.10>.
- [17] M. A. Adam, A. M. Erfan, F. A. Habib, and T. A. El-Sayed, "Structural Behavior of High-Strength Concrete Slabs Reinforced with GFRP Bars," *Polymers*, vol. 13, no. 17, Jan. 2021, Art. no. 2997, <https://doi.org/10.3390/polym13172997>.
- [18] H. A. Hasan, H. Karim, H. A. Goaz, A. M. Cabe, M. N. Sheikh, and M. N. S. Hadi, "Performance evaluation of normal- and high-strength concrete column specimens reinforced longitudinally with different ratios of GFRP bars," *Structures*, vol. 47, pp. 1428-1440, Jan. 2023, <https://doi.org/10.1016/j.istruc.2022.11.056>.
- [19] S. A. Mohammed and A. I. Said, "Analysis of concrete beams reinforced by GFRP bars with varying parameters," *Journal of the Mechanical Behavior of Materials*, vol. 31, no. 1, pp. 767-774, Jan. 2022, <https://doi.org/10.1515/jmbm-2022-0068>.
- [20] A. Said and O. M. Abbas, "Evaluation of Deflection in High Strength Concrete (HSC) I-beam Reinforced with Carbon Fiber Reinforced Polymer (CFRP) Bars," in *The 7th Asia Pacific Young Researchers and Graduates Symposium*, Kuala Lumpur, Malaysia, Aug. 2015, pp. 519-533.
- [21] A. Ramachandra Murthy, DM. Pukazhendhi, S. Vishnuvardhan, M. Saravanan, and P. Gandhi, "Performance of concrete beams reinforced with GFRP bars under monotonic loading," *Structures*, vol. 27, pp. 1274-1288, Oct. 2020, <https://doi.org/10.1016/j.istruc.2020.07.020>.
- [22] S. I. Ali and A. A. Allawi, "Effect of Web Stiffeners on The Flexural Behavior of Composite GFRP- Concrete Beam Under Impact Load," *Journal of Engineering*, vol. 27, no. 3, pp. 76-92, Feb. 2021, <https://doi.org/10.31026/j.eng.2021.03.06>.
- [23] A. W. Naqe and A. H. Al-zuhairi, "Strengthening of RC Beam with Large Square Opening Using CFRP," *Journal of Engineering*, vol. 26, no. 10, pp. 123-134, Oct. 2020, <https://doi.org/10.31026/j.eng.2020.10.09>.
- [24] M. Y. Alabdulhady, M. F. Ojaimi, and A. H. Chkheiw, "The efficiency of CFRP strengthening and repair system on the flexural behavior of RC beams constructed with different concrete compressive strength," *Results in Engineering*, vol. 16, Dec. 2022, Art. no. 100763, <https://doi.org/10.1016/j.rineng.2022.100763>.
- [25] M. Issa, A. Allawi, and N. Oukaili, "Performance of doubly reinforced concrete beams with GFRP bars," *Journal of the Mechanical Behavior of Materials*, vol. 33, Jan. 2024, Art. no. 20220308, <https://doi.org/10.1515/jmbm-2022-0308>.
- [26] T. H. Ibrahim, A. A. Allawi, and A. El-Zohairy, "Experimental and FE analysis of composite RC beams with encased pultruded GFRP I-beam under static loads," *Advances in Structural Engineering*, vol. 26, no. 3, pp. 516-532, Feb. 2023, <https://doi.org/10.1177/13694332221130795>.
- [27] H. Falah, Ibrahim, and A. Al-Ahmed, "Strengthening of Cracked One-Way Reinforced Concrete Bubbled Slabs using External Strands," *Design Engineering*, vol. 3, pp. 60-78, Mar. 2021.
- [28] R. Mathew and P. Binu, "CFRP Strips on Punching Shear Strength Development of Bubble Deck Slab," *International Journal of Advanced Research Trends in Engineering and Technology*, vol. 2, no. 9, pp. 1-5, 2015.
- [29] J. Jamal and V. Vijayan, "A Study on Strengthening of Bubble Deck Slab With Elliptical Balls by Using GFRP Sheets," *International Journal for Scientific Research & Development*, vol. 6, no. 1, pp. 659-663, 2018, <https://doi.org/10.2139/ssrn.3591289>.
- [30] W. D. Salman, "Flexural behavior of bubbled reinforced concrete slabs," Ph.D. dissertation, University of Baghdad, Baghdad, Iraq, 2012.
- [31] W. A. Waryosh and H. H. Hashim, "Rehabilitation of Fire Damage Reinforced Concrete Bubbled Slabs," *Journal of Global Scientific Research*, vol. 1, pp. 278-288, 2020.
- [32] S. S. Aman, B. S. Mohammed, M. A. Wahab, and A. Anwar, "Performance of Reinforced Concrete Slab with Opening Strengthened Using CFRP," *Fibers*, vol. 8, no. 4, Apr. 2020, Art. no. 25, <https://doi.org/10.3390/fib8040025>.
- [33] K. Attia, W. Alnahhal, A. Elrefai, and Y. Rihan, "Flexural behavior of basalt fiber-reinforced concrete slab strips reinforced with BFRP and GFRP bars," *Composite Structures*, vol. 211, pp. 1-12, Mar. 2019, <https://doi.org/10.1016/j.compstruct.2018.12.016>.
- [34] R. Shamass and K. A. Cashell, "Experimental investigation into the flexural behaviour of basalt FRP reinforced concrete members," *Engineering Structures*, vol. 220, Oct. 2020, Art. no. 110950, <https://doi.org/10.1016/j.engstruct.2020.110950>.

-
- [35] S. H. Al-Tersawy and M. A. Ghanem, "Ductility and Flexural Behavior of One Way Concrete Slabs Reinforced With Local Gfrp Rebars: an Experimental and Analytical Study," *Engineering Research Journal*, vol. 37, no. 1, pp. 95–106, Jan. 2014, <https://doi.org/10.21608/erjm.2014.66873>.
- [36] ACI440.1R-15, *Guide for the Design and Construction of Structural Concrete Reinforced with Fiber-Reinforced Polymer (FRP) Bars*. Farmington Hills, MI, USA: American Concrete Institute, 2015.
- [37] A. A. Al-Azzawi and S. H. Mtashar, "Behavior of two-way reinforced concrete voided slabs enhanced by steel fibers and GFRP sheets under repeated loading," *Results in Engineering*, vol. 17, Mar. 2023, Art. no. 100872, <https://doi.org/10.1016/j.rineng.2022.100872>.